

Effect of rock discontinuities on certain rock strength and fracture energy parameters under uniaxial compression

C.E. TSOUTRELIS and G.E. EXADAKTYLOS

Department of Mining Engineering, National Technical University of Athens, 42 Patission Street, Athens 10682, Greece

Received 4 January 1991

Summary

Five series of test blocks of Pendeli marble with artificially created discontinuities of different crack densities (simulating three mutually orthogonal joint sets) were tested in uniaxial compression in order to study the effect of discontinuities on: (a) the compressive strength and the modulus of elasticity, and (b) certain fracture energy parameters expressed by the ratio W_A/W_V , where W_A is the surface energy and W_V the volume elastic strain energy. Mathematical relationships are derived similar to those suggested by other authors relating strength parameters to crack densities. Such relationships clearly show a reduction in strength with increased crack density. The experimental results obtained permit the extension of Persson's relation (which refers to ideal intact rock) to the more realistic case of discontinuous rock mass by introducing the appropriate term that takes into consideration the effect of rock mass discontinuities on the energy ratio W_A/W_V . A comparison between laboratory results and field observations was subsequently carried out assuming the rock mass to behave as a linearly elastic material, obeying the Hoek and Brown failure criterion. This comparison showed that laboratory results can be extended to larger scale. Furthermore, in order to predict the *in situ* strength and stability of a rock mass in uniaxial compression (which is of major importance in underground excavations) certain concepts are proposed based on laboratory tests, *in situ* investigations and first principles of linear elastic fracture mechanics.

Keywords: Rock discontinuities; uniaxial compression; fracture mechanics; stability; scale effect.

Introduction

It is generally recognized that rock discontinuities affect the strength properties of rock masses, and many examples can be cited from the relevant literature of rock failure due to the misjudgement of the effect of discontinuities on rock strength. Griffith's (1921) theoretical criterion of brittle failure is based on the assumption of the presence of microcracks in the rock, while the empirical criterion of failure of Hoek and Brown (1980) includes two strength parameters that depend on the discontinuities present in the rock mass.

This paper examines the effect of artificially created discontinuities in rock blocks of different crack densities on the compressive strength, the modulus of elasticity and on certain fracture energy parameters. The scale dependence of rock strength and post-peak stability of the discontinuous rock is also investigated.

Selection of rock type

A careful examination of different rock types available for experimentation led to the conclusion that the white marble of Pendeli was a good selection for the construction of the test blocks and for field validation of the laboratory results, since an operating quarry with good exposures was accessible. Pendeli marble, which was used by the Athenians to build the Parthenon, is a rock virtually free from visible cracks; it is homogeneous, isotropic and practically linear elastic to failure, thus approaching the ideal intact rock to which linear elastic fracture mechanics (LEFM) theory can be applied. This marble consists of an equidimensional mosaic of fine calcite grains (Roos *et al.*, 1988) with straight to gently curved boundaries having an average size of 0.2 mm. Certain of its properties are given in Table 1. Furthermore, the statistical homogeneity of the intact rock material has been confirmed indirectly from uniaxial compressive test data. It should be expected, therefore, that in such a rock any difference in its behaviour during the experimental procedure can be attributed to the artificially created discontinuities and not to other factors.

Table 1. Mineral content, grain size and certain mechanical properties of Pendeli marble

Calcite	99%
Quartz	<1%
Grain size	<1 mm
Specific gravity	$2.70 (\times 10^5 \text{ N m}^{-3})$
Porosity	0.371%
Compressive strength	83 MPa
Tensile strength	12 MPa
Modulus of elasticity	12 GPa

Experimental procedure

Three mutually orthogonal rock discontinuity sets in the test blocks were simulated by bonding together marble pieces of specific sizes using a low-strength marble glue in order to create prismatic blocks $60 \times 60 \times 80$ mm in size, each one having a different percentage of artificially created discontinuities. This difference was expressed quantitatively by the crack density factor f of each test block in square metres of discontinuity surfaces per cubic metre of test block (m^2/m^3). Gluing was necessary in order to create the necessary cohesion between the marble pieces of each block and to assist in grinding the opposite block faces to the prescribed standards set by ISRM (Brown, 1981). Five series, each of five test blocks as shown in Fig. 1, were constructed having crack density factors varying from $f=0$ (A1) to $f=104 \text{ m}^2/\text{m}^3$ (A5). The test blocks were subsequently fractured in uniaxial compression

using an SBEL CT-250A loading machine under a loading rate of 0.7 MPa s^{-1} according to the ISRM suggested procedure (Brown, 1981). The axial deformation of each test block was recorded by a dial gauge to within 0.001 mm.

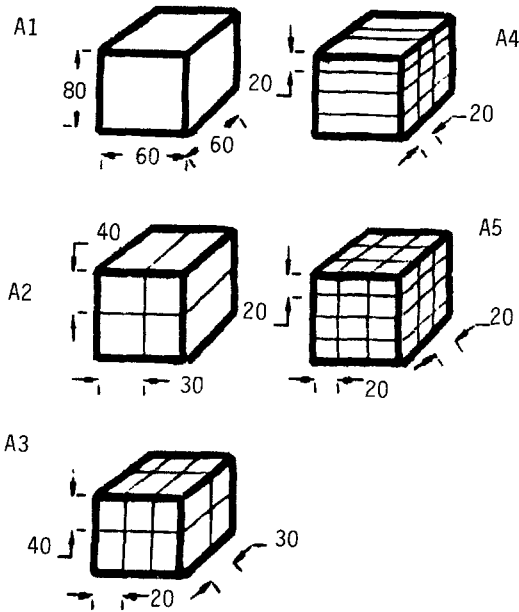


Fig. 1. Test specimens A1–A5 of Pendeli marble. Artificial discontinuities in specimens A2–A5 are shown in thin lines (all dimensions in mm)

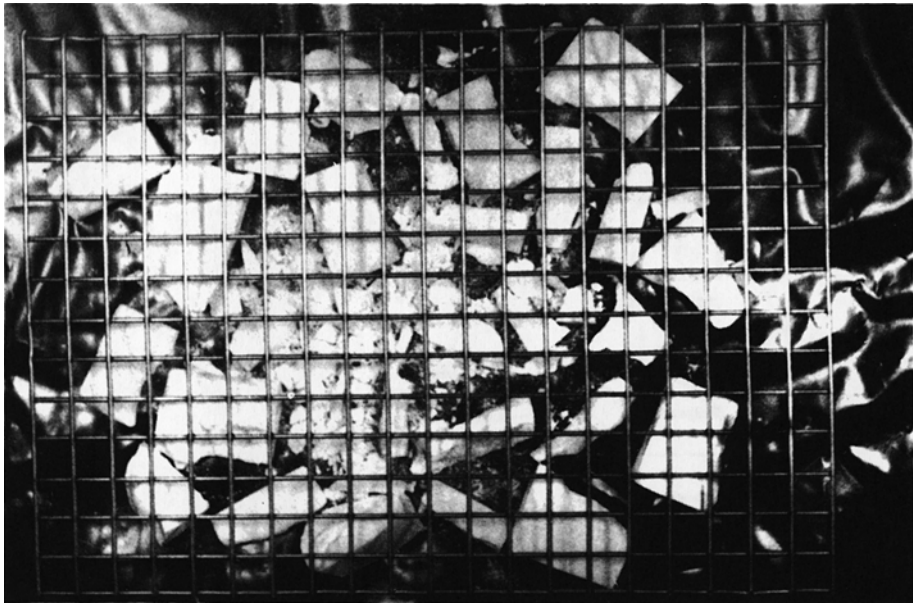
The total surface area A created during fracturing in each test block was estimated using Herdan's formula (Herdan, 1960) after establishing the fragment size distribution by sieving and characterizing their shapes by an appropriate shape factor (see Appendix A). The method used to determine the shape factor K of the fragments was as follows.

- (1) After each test, the fragments were laid on a flat surface and the reference grid shown in Fig. 2a was superimposed on them.
- (2) Next, the fragments with the superimposed grid were photographed and the photographs taken were digitized in a computer (Fig. 2b) to characterize numerically the geometrical shape of the fragments (expressed by the maximum and minimum dimension of the fragments).

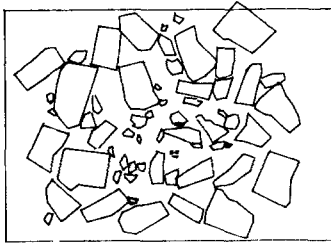
Any cracks present which were visible to the eye in the relatively large fragments, and which were not considered by Herdan's formula, were measured separately and added to those estimated previously.

Effect of the crack density factor on the strength parameters

Typical axial load–axial displacement curves for the five series of test blocks are shown in Fig. 3. The following parameters were measured from the relevant tests.



(a)



(b)

0.1 cm

Fig. 2. Numerical characterization of the geometrical shape of fragments produced after each test: (a) photograph; (b) digitized photograph

- (1) the uniaxial compressive strength σ_c , which was obtained by dividing the peak load carried by the specimen during the test by the initial cross-sectional area of the specimen;
- (2) the tangent modulus of elasticity E , measured at a stress level equal to $0.5 \sigma_c$;
- (3) the fragment size distribution produced after fracturing;
- (4) for the test blocks of series A3, A4 and A5, for which the full failure curves were obtained, the area under the axial load–axial deformation curves, as depicted in Fig. 4. In terms of energy this area represents the surface energy W_A absorbed during the propagation of cracks in the rock until complete failure.

The mode of failure of the intact marble test blocks (A1) was manifested by a system of conjugate shear cracks and crushing at late stages of compression. The photographs of Fig. 5 show early and intermediate stages in the compression of test blocks A2 which contain artificial discontinuities. The mode of failure is manifested by a system of both linear and curved cracks running in an oblique direction to the direction of loading and across the horizontal artificial discontinuity of the test block. This indicates that the effect of pre-

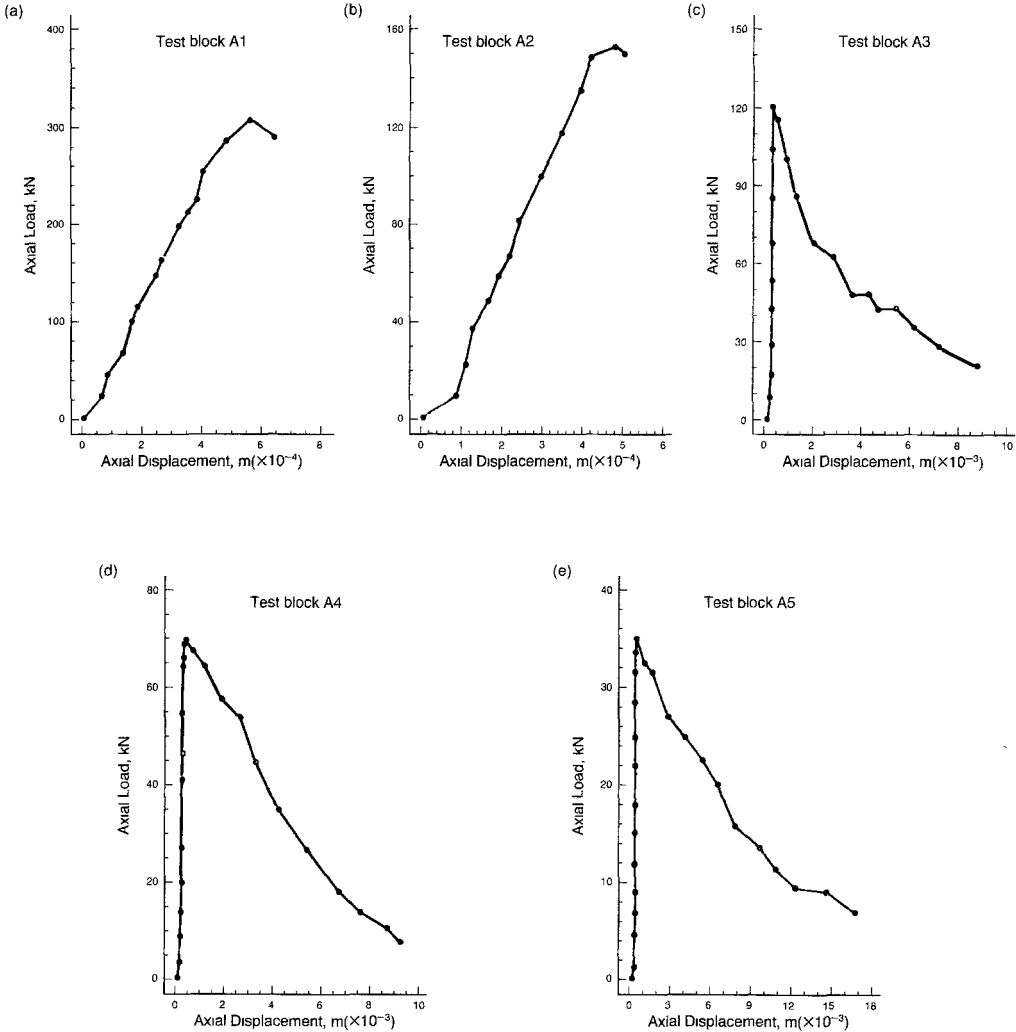


Fig. 3. Typical load–deformation curves for the five types of test block (the circles denote experimental points). Note different horizontal scales for (a) and (b)

existing artificial discontinuities is to create a rather more complicated crack pattern than the single system of conjugate shear cracks created in the intact specimen.

The experimental results for the variation of the compressive strength σ_c and of the modulus of elasticity E with respect to different crack densities values f are summarized in Tables 2 and 3. The indices d and i denote test blocks with and without artificially created discontinuities respectively. From Tables 2 and 3 it can be seen that the dispersion of the values of the uniaxial compressive strength and of the modulus of elasticity around the mean value was not significant for each of the five series of the test blocks. This implies that the intact rock material used in the experiments is statistically homogeneous.

As expected, the effect of rock discontinuities was to reduce the rock strength and the elastic parameters. Such reduction is expressed for the case under consideration by the following relationships, which are graphically shown in Figs 6 and 7 respectively:

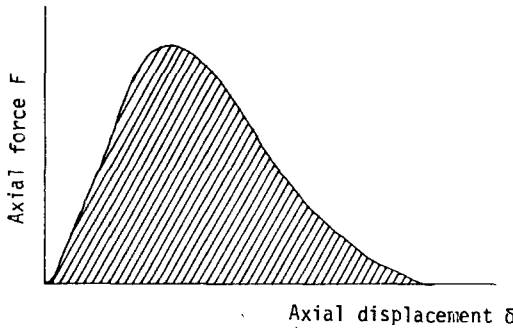


Fig. 4. Complete load–deformation curve of a linearly elastic softening material. The area under this curve represents, in terms of energy, the surface energy dissipated during crack propagation

$$\frac{\sigma_{cd}}{\sigma_{ci}} = e^{-0.0187f} \quad (1)$$

$$\frac{E_d}{E_i} = e^{-0.0124f} \quad (2)$$

Since in the present experiments the edge-length of all the nearly cubical specimens, L_s , was constant and equal to 0.06 m, then by considering geometric similarity principles in order to apply the previous equations to other sizes L and corresponding crack density factors f , the following are obtained:

$$\frac{\sigma_{cd}}{\sigma_{ci}} = e^{-0.0187(L/L_s)f} \quad (3)$$

$$\frac{E_d}{E_i} = e^{-0.0124(L/L_s)f} \quad (4)$$

with $L_s = 0.06$ m.

Energy parameters related to fracture of intact rocks

Progress made during recent years in the fields of experimental observation and fracture mechanics permits further examination of the effect of artificially created discontinuities on certain energy parameters related to fracture. For this examination the energy ratio W_A/W_V was selected which is also referred to in the literature as ‘brittleness number’ (Cherepanov, 1979; Carpinteri, 1980), where W_A is the surface energy and W_V is the volume elastic strain energy. The former is the energy consumed within the rock during the pre-failure and post-failure regime of the test block in order to gradually extend pre-existing cracks and to create new surfaces. The consumption of this energy increases as the stress level increases, since more cracks are activated and new surfaces are created that finally lead to rock failure by fracture. According to Ouchterlony (1980) W_A is related to the total surface area A of newly created cracks in the rock by the relationship:

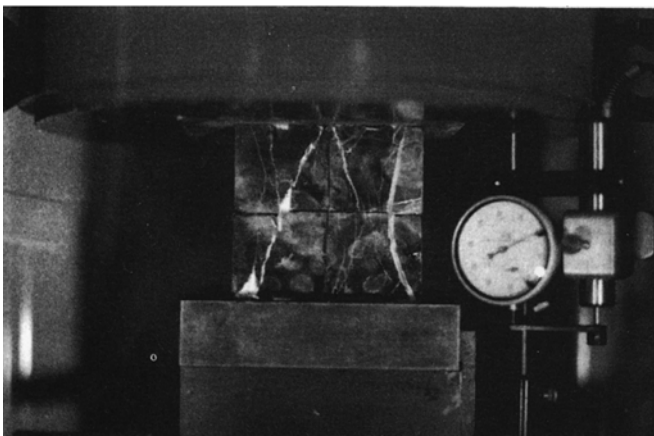
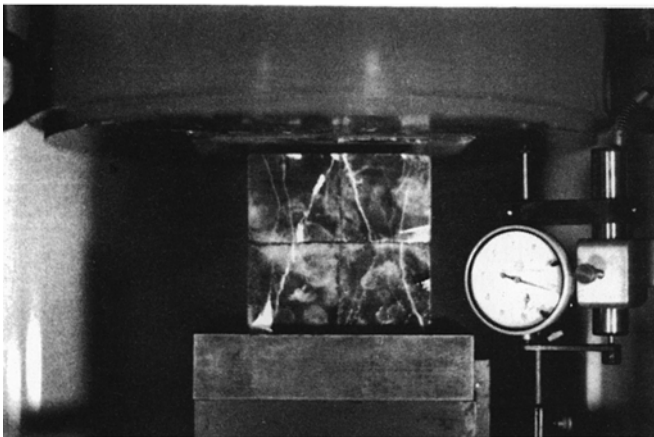
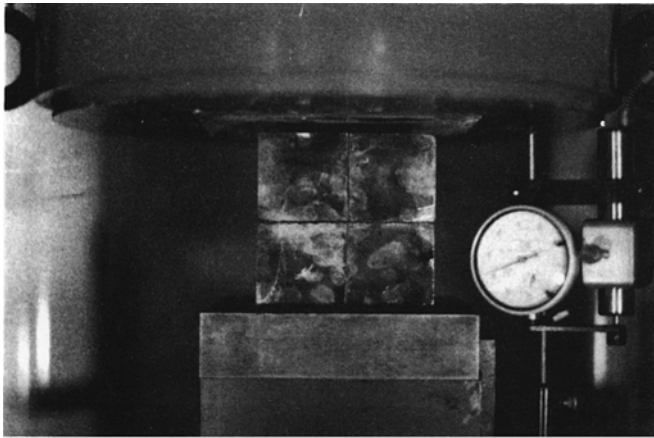


Fig. 5. Progressive failure of a marble specimen with artificial discontinuities (test block A2)

Table 2. Effect of the crack density factor f of artificial discontinuities on the uniaxial compressive strength σ_c

Test block	Crack density factor, f (m^2/m^3)	σ_c mean value (MPa)	Standard deviation of σ_c (MPa)	$\sigma_{cd}/\sigma_{ci}^a$
A1	0	83.00	8.45	1.00
A2	29	43.99	5.40	0.53
A3	50	37.35	5.95	0.45
A4	71	21.58	5.63	0.26
A5	104	10.79	3.80	0.13

^a σ_{cd} , UCS for blocks with discontinuities introduced; σ_{ci} , UCS for intact blocks.

Table 3. Effect of the crack density factor f of artificial discontinuities on the modulus of elasticity E

Test block	Crack density factor, f (m^2/m^3)	E mean value (GPa)	Standard deviation of E (GPa)	E_d/E_i^a
A1	0	12.00	2.44	1.00
A2	29	7.80	1.36	0.65
A3	50	6.96	1.39	0.58
A4	71	4.56	1.33	0.38
A5	104	3.60	0.87	0.30

^a E_d , modulus of elasticity for blocks with discontinuities introduced; E_i , modulus of elasticity for intact blocks.

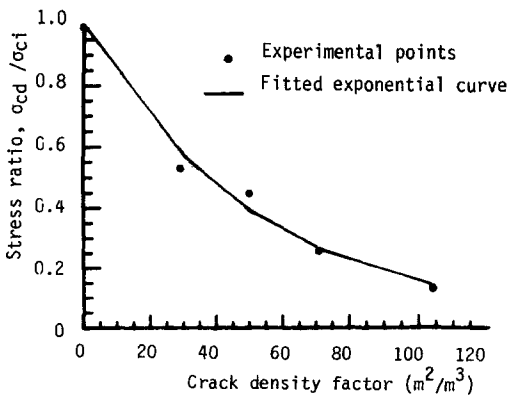


Fig. 6. Effect of crack density factor on the stress ratio σ_{cd}/σ_{ci}

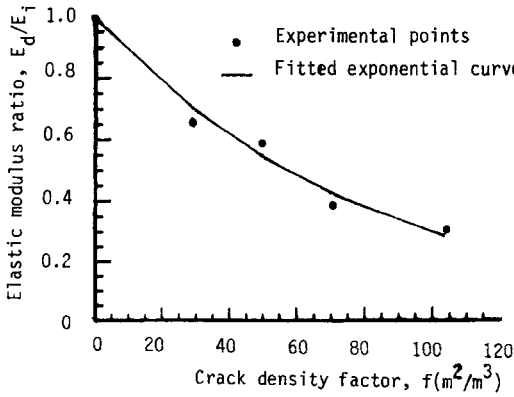


Fig. 7. Effect of crack density factor on the modulus ratio E_d/E_1

$$W_A = \gamma A \quad (5)$$

where W_A is expressed in joules, A in m^2 and γ is the specific surface energy expressed in $J m^{-2}$. γ represents the surface energy consumed per unit area of the newly created crack surfaces and depends on the specific material response during the fracture process under consideration. When the fracture mechanism is perfectly brittle, γ can be estimated either from atomic force attraction laws or from measurements. If, however, energy is irreversibly dissipated through plastic flow or through another dissipative mechanism (such as friction) during a unit area crack extension, then the specific surface energy is referred to as the effective specific surface energy Γ and includes the true surface free energy γ plus all the other forms of dissipative energies, which sometimes considerably surpass the former. Krech and Chamberlain (1972) demonstrated experimentally that Γ is between 140 and 560 times higher in a uniaxial compressive test than in a uniaxial tensile test, with the higher values noted in strong materials like Barre granite, and the lower in weaker materials like Berea sandstone. Also, Kemeny and Cook (1987) found from compression experiments that for Westerly granite, the energies to create splitting and shear cracks are about three orders of magnitude greater than the energy needed to drive the tensile microcracks, owing to the large amount of subsidiary crack surface area created in forming the larger-scale fractures. Labuz and Biolzi (1991) found from triaxial test data that $\Gamma = 2000 J m^{-2}$ for Indiana limestone while the tensile specific surface energy γ of the same rock was found to be equal to $0.035 J m^{-2}$.

Therefore, from an engineering point of view, an experimentally measured value of Γ is preferred. This can be done by measuring the area under the axial load–axial displacement curve obtained using a servo-controlled or stiff loading machine (Krech and Chamberlain, 1972), as shown in Fig. 4. From the experimental data from test blocks A3, A4 and A5, for which the full failure curves were obtained, Table 4 was constructed. From this table the following conclusions can be drawn.

- (1) The effective specific surface energy Γ is not much affected by the crack density factor f of the artificial discontinuities (coefficient of variation = 8.5%).
- (2) The mean value of Γ can be taken as $4340 J m^{-2}$. Since in bending tests under three-point loading on prenotched marble specimens described in Appendix B, γ was

Table 4. Effect of the crack density factor f of artificial discontinuities on the effective specific surface energy Γ

Test block	Crack density factor, f (m^2/m^3)	Γ mean value (J m^{-2})	Standard deviation of Γ (J m^{-2})
A3	50	4755	571
A4	71	3856	694
A5	104	4403	616

found to be equal to 44 J m^{-2} , it is concluded that the effective specific surface energy in compression, Γ , is 98.6 times the specific surface energy in tension, γ .

The other energy parameter W_V is the elastic strain energy which has been stored in the strained rock until the peak load point is reached. It is proportional to the volume of the test block and is represented by the area under the prefailure portion of the axial load–axial displacement curve. For the case under consideration of uniaxial compression of a linearly elastic Hookean material the following relationship holds true (Jaeger and Cook, 1976):

$$W_V = \frac{\sigma_c^2}{2E} V_0 \quad (6)$$

where W_V is the stored elastic strain energy in rock of volume V_0 (J), σ_c is the compressive strength (N m^{-2}), E is the modulus of elasticity (N m^{-2}), and V_0 is the initial volume of the rock specimen tested (m^3).

Persson (1983) studied in detail the variation of the energy ratio with respect to the mode of loading, the geometric size and certain mechanical properties of rocks. He concluded that for the case of linearly elastic, brittle and intact rock subjected to uniaxial loading, the ratio W_A/W_V at fracture is given by

$$\left(\frac{W_A}{W_V}\right)_i = \frac{2E\Gamma A}{\sigma_{ci}^2 V_0} = \frac{Cr_Y}{L} \quad (7)$$

where C is a constant depending on the nature of the crack tip stress field and the geometry of rock fracture (axial splitting or shear band type of fracture), r_Y is the characteristic size of the microcracking zone ahead of the crack tip (m), and L is the characteristic dimension of the rock structure or specimen (m).

The characteristic microcracking zone size can be regarded as an adjustment term to be added to the notch depth or the crack depth in LEFM calculations or in the evaluation of experimental results. Based on LEFM theory the characteristic size of the microcracking process zone can be estimated (Ouchterlony, 1980) by the relationships

$$r_Y = \frac{0.4E\gamma}{\sigma_t^2} \quad (8)$$

or

$$r_Y \cong \frac{0.2K_{IC}^2}{\sigma_t^2} \quad (9)$$

since $K_{IC} = (2E\gamma)^{1/2}$, where E is the modulus of elasticity (N m^{-2}), σ_t is the tensile strength of rock (N m^{-2}), and K_{IC} is the critical mode-I stress intensity factor in plane strain conditions or fracture toughness of the rock ($\text{N m}^{-3/2}$).

The tensile strength of Pendeli marble was determined by the Brazilian test according to ISRM (1978) specifications. From these tests a mean value of $\sigma_t = 12$ MPa with a standard deviation of 0.7 MPa was obtained. Fracture toughness K_{IC} was also determined experimentally by testing prenotched marble specimens in three-point bending as is described in detail in Appendix B. K_{IC} and γ were found to be equal to $1.03 \text{ MN m}^{-3/2}$ and 44 J m^{-2} respectively.

Having estimated K_{IC} and σ_t , then from Equation 9 we get

$$r_Y = 0.002 \text{ m}$$

For the uniaxial compression of intact Pendeli marble test blocks, the constant parameter C of Equation 7 can be estimated by inserting the following values in the equation:

$$\Gamma = 98\gamma$$

$$\sigma_c = \frac{83}{12}\sigma_t$$

$$\frac{A}{V_0} = 53L_s^{-1} \left(\frac{L_s}{L} \right) = 53L^{-1}$$

and by taking into account Equation 8 the following is obtained:

$$\left(\frac{W_A}{W_V} \right)_i = \frac{0.4E\gamma}{\sigma_t^2} \frac{2}{0.4} \frac{98}{\left(\frac{83}{12}\right)^2} \frac{53}{L} = 543 \frac{r_Y}{L} \quad (10)$$

Therefore $C = 543$ in the case under consideration. This value is 3.6 times higher than the value of C reported by Persson (1983), namely $C = 150$. This can be attributed to the fact that the growth of one macrofracture at an angle β with respect to the loading direction assumed by Persson (1983) has been replaced in the intact marble test blocks by a system of conjugate shear cracks at the peak load and later crushing of the specimen in the post-failure regime that results in the creation of a greater surface area than that of Persson's macrofracture.

Equations 7 and 10, however, which hold true for the intact rock with Griffith cracks, do not take into consideration the effect of pre-existing macro-discontinuities in the ratio W_A/W_V and consequently they cannot be applied to jointed rock masses.

Effect of the crack density factor on the energy and strength parameters

Laboratory-scale analysis

Present experiments permit the extension of the energy relationship (Equation 8) to the discontinuous rock material domain provided that measurements of the newly created surfaces can be established up to the point of fracture. Following Herdan's (1960) relation the new surfaces created in each test block until fracture occurred in uniaxial compression were established by sieving and weighing. The results are given in Table 5 and presented diagrammatically in Fig. 8. The variation of the ratio A_d/A_i with respect to the crack density

Table 5. Effect of the crack density factor f of artificial discontinuities on the newly created area of fracture surfaces, A

Test block	Crack density factor, f (m^2/m^3)	A mean value (m^2)	Standard deviation of A (m^2)	A_d/A_i^a
A1	0	0.190	0.037	1.00
A2	29	0.140	0.029	0.73
A3	50	0.120	0.034	0.63
A4	71	0.100	0.016	0.54
A5	104	0.074	0.024	0.39

^a A_d , area of fracture surfaces for blocks with discontinuities introduced; A_i , area of fracture surfaces for intact blocks

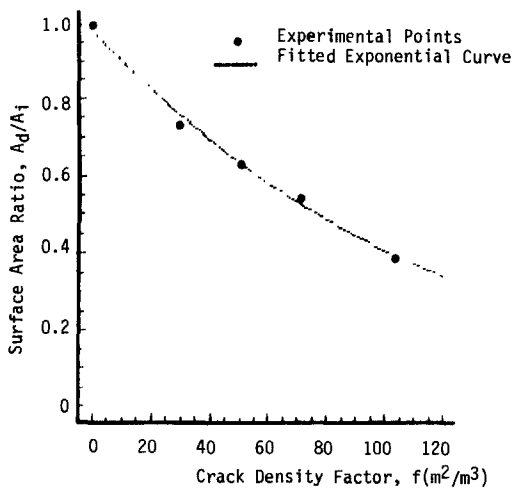


Fig. 8. Effect of crack density factor on the surface area ratio A_d/A_i

factor f is given by the following equation, which was derived by nonlinear regression analysis of the experimental data at 95% confidence level:

$$\frac{A_d}{A_i} = e^{-0.0194(L/L_s)f}, \quad \text{for } L_s = 0.06 \text{ m} \quad (11)$$

The above equation shows that as the crack density factor of the artificially created discontinuities increases in the test block and the compressive strength decreases, a reduction of the newly formed cracks during fracturing is observed. This observation agrees with the theoretical model of brittle fracture and the experimental results of Radchenko and Michailov (1970) and Shukla and Fourney (1983). It is due to the fact that the ability of the rock to store strain energy decreases as the density of pre-existing discontinuities increases.

By dividing the first term of Equation 7 for discontinuous and intact rock, the following relationship is obtained:

$$\frac{(W_A/W_V)_d}{(W_A/W_V)_i} = \frac{E_d}{E_i} \left[\frac{\sigma_{cd}}{\sigma_{ci}} \right]^{-2} \frac{A_d \Gamma_d}{A_i \Gamma_i} \quad (12)$$

Equation 12 coupled with the previous Equations 3, 4, 7 and 11 and the experimental observation that Γ values are not much affected by the presence of discontinuities (i.e. $\Gamma_d = \Gamma_i = \Gamma$) suggest that the following general empirical equation relates the energy ratio to certain fracture mechanics properties of the rock mass:

$$\frac{W_A}{W_V} = \frac{Cr_Y}{L} e^{\alpha(L/L_s)f} \quad (13)$$

where in the example considered the constant parameters are: $\alpha = 0.018$ m, $C = 543$, $r_Y = 0.002$ m and $L_s = 0.06$ m. The value of α is characterized by a length dimension due to dimensional considerations. Equation 13 is an extension of Equation 7 derived by Persson for intact rock. The term $e^{\alpha(L/L_s)f}$ appearing in Equation 13 is a configuration correction factor experimentally derived that takes into account the effect of pre-existing discontinuities, as well as the scale effect, on the energy ratio. Although the size of the microcracking process zone r_Y is affected by the presence of discontinuity surfaces, as LEFM predicts, in the above formulation this effect is discarded since r_Y in Equation 13 is related only to the ratio $(W_A/W_V)_i$ in the left term of Equation 12; that is, it is a property of the intact rock only.

Extrapolation of laboratory results to larger scale

Since Equation 13 was derived from laboratory experiments, it is interesting to know if its validity can be extended to *in situ* rock masses and for ranges of f -values other than those artificially created.

Based on (a) back analysis of the rock mass strength from a number of studies of *in situ* plate bearing tests on rock specimens of size L of the order of 0.5 m, and (b) on the Hoek and Brown criterion of failure of rock masses, Brown and Hoek (1988) and Nicholson and Bieniawski (1990) suggested the following relationships:

$$\frac{\sigma_{cd}}{\sigma_{ci}} = e^{(RMR - 100)/18} \quad (14a)$$

$$\frac{E_d}{E_i} = (1/t)e^{(RMR - 100)/18} \quad (14b)$$

where RMR is the rock mass rating, varying from very low values for completely fractured rocks to 100 for the intact rock, and t is a scale parameter which varies between 1.0 for intact rock with RMR = 100 and some upper bound value for completely fractured rock with RMR = 0.

In order to compare the strength ratios predicted from Equations 14a and 3 the RMR value is substituted by the joint spacing rating (JSR) based on the following relations (Bieniawski, 1976):

$$RMR = 70 + JSR \quad \text{for} \quad JSR > 10 \quad (15a)$$

$$RMR = 53 + JSR \quad \text{for} \quad JSR \leq 10 \tag{15b}$$

Therefore, Equation 14 becomes:

$$\frac{\sigma_{cd}}{\sigma_{ci}} = e^{(JSR - 30)/18} \quad \text{for} \quad JSR > 10 \tag{16a}$$

$$\frac{\sigma_{cd}}{\sigma_{ci}} = e^{(JSR - 47)/18} \quad \text{for} \quad JSR \leq 10 \tag{16b}$$

Since in the plate bearing tests $L = 0.5$ m then the corrected Equation 3 for this scale becomes

$$\frac{\sigma_{cd}}{\sigma_{ci}} = e^{-0.187f} \tag{17}$$

with $f = (\text{joint spacing})^{-1}$ according to geometrical probability principles (Underwood, 1968). The strength ratios σ_{cd}/σ_{ci} predicted from Equations 16 and 17 for various values of f and corresponding values of JSR are compared in Table 6. It can be easily concluded that they are in agreement except for a highly fractured rock mass, where Equation 17 gives a lower strength ratio.

Table 6. Comparison of the ratio σ_{cd}/σ_{ci} values obtained using the Brown and Hoek (1988) relation and Equation 17

Crack density factor, f (m^2/m^3)	JSR	σ_{cd}/σ_{ci} ^a	
		Brown and Hoek (1988) Equation 16	Equation 17
0.33	30	1.00	0.94
1.00	25	0.75	0.83
3.33	20	0.57	0.54
20.00	10	0.13	0.02

^a σ_{cd} , UCS for blocks with discontinuities introduced; σ_{ci} , UCS for intact blocks.

Since Γ was found to be independent of f in the uniaxial compression of the marble test blocks, and assuming that this holds true irrespective of the testing scale, it only remains to be shown that the ratio A_d/A_i is exponentially related to f , in order that Equation 10 can be taken to apply to the loading conditions of the rock mass of Pendeli marble. To investigate this relationship, for which no data exist in literature, a large three-dimensional exposure of Pendeli marble at a quarry face was selected and site investigations were carried out in order to distinguish between primary and secondary discontinuities of the rock mass as discussed below.

It was found that three orthogonal discontinuity sets of high persistence were present in the rock mass: one set belonging to bedding, and two others to axial splitting joint sets. The joints were characterized by fairly smooth, planar surfaces, continuity in orientation and infilling with hard calcite or ferruginous material. This discontinuity pattern, which reflects the local geology and early tectonics, is considered as primary. It was similar to the three

mutually orthogonal joint sets simulated in the marble test blocks of our experiments. A total number of four sampling windows of fresh marble exposures in the same quarry face having an L dimension equal to 6 m and different intensity of pre-existing discontinuities were photographed. The discontinuity patterns present in the photographs were then computer digitized. These sampling windows were considered to represent typical two-dimensional sections of corresponding rock blocks in the rock mass with the third dimension of 1 m, which corresponds to the mean spacing of the third joint set. Since each of the exposed planes appearing in the photographs corresponds to one of the pre-existing joint sets, two pre-existing discontinuity sets of the rock were present in the digitized photographs as is shown in Fig. 9. The remaining joints and cracks appearing in the photographs were the result of compressive strain episodes of later age as witnessed by branching, rough surfaces, small apertures, non-persistence and random orientation with some of the joints following the orientations of the primary joint sets. These were considered as secondary discontinuities.

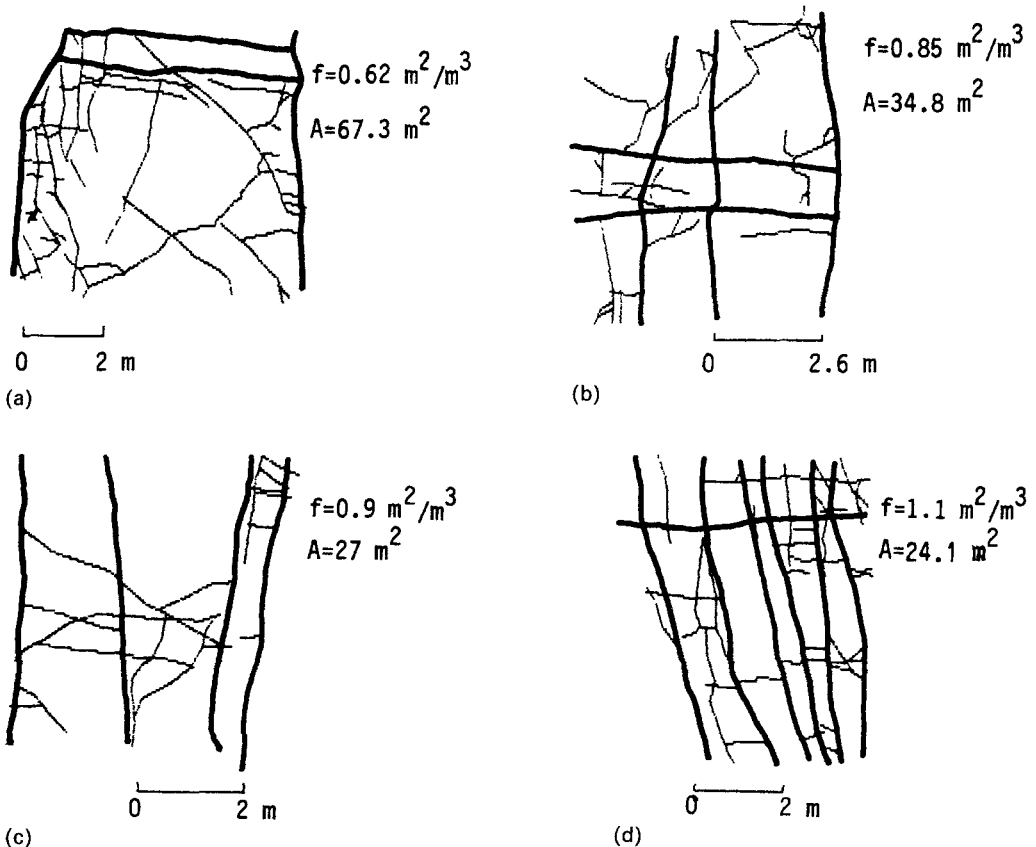


Fig. 9. Digitized photographs of exposed Pendeli marble surfaces of different crack density factors (appearing darker and thicker than the secondary cracks)

From the digitized photographs (Fig. 9) the average spacing S_{av} of the new (secondary) discontinuities on a superimposed set of perpendicular sampling lines was found and the corresponding total surface area (opposite sides of the crack surface areas are both considered) was estimated by the relation (Underwood, 1968)

$$A = \frac{2V}{S_{av}} \quad (18)$$

where V is the volume of the rock block corresponding to the digitized photograph ($6 \times 6 \times 1 = 36 \text{ m}^3$).

Since the pre-existing (primary) discontinuities were persistent, then their specific trace length per unit area of the digitized photograph is equal to their specific surface area f (m^2/m^3). By using a simple regression analysis, the following exponential relationship was found between f and the ratio A_d/A_i at 95% confidence level and correlation coefficient $R=0.9662$:

$$\frac{A_d}{A_i} = e^{-2.23f} \quad (19)$$

By comparing Equations 11–19 it can be concluded that laboratory-scale results are extended to full-scale loading of the *in situ* rock mass since, from Equation 11, the multiplication factor of f is equal to $-(6/0.06) \times 0.0194$ or -1.94 as compared with -2.23 from actual field measurements.

It was shown previously that the strength and the new crack surface area ratios derived from the laboratory-scale tests Equations 14a and 19 can be extrapolated to the *in situ* rock mass. The same conclusion, however, cannot be made for the modulus of elasticity ratio since the distribution of the scale parameter t appearing in Equation 14b is not known. By considering that

- (1) Equation 14b proposed by Nicholson and Bieniawski shows that the elasticity ratio is an exponential function of RMR, or according to geometrical probability principles an exponential function of f (Underwood, 1968),
- (2) the new crack surface areas created during rock fracturing depend both on σ_c and E according to fundamental physical laws, and
- (3) the new crack surface area and strength ratios can be extended to larger scales,

it can be concluded indirectly that the modulus of elasticity ratio given by Equation 4 is also valid for larger scales. Furthermore, the exponential relationship in Equation 13 for the energy ratio can be extrapolated to larger scales since from Equation 12 all the ratios appearing in the right-hand side of the same relationship can be extended to larger scales.

Scale effect on rock mass strength and stability

The size effect on failure load and on stability denotes a decrease of the stress at failure and a change in the mode of stability respectively, when the size of geometrically similar rock structures or of specimens under the same loading conditions increases. Based on the previous considerations the scale effect on strength and stability of discontinuous rock masses can be assessed. The approach of Berry (1960) and Cook (1965) is followed and not that of statistical fracture mechanics theory (Weibull, 1939), since the major assumption of this theory is that only the distribution of flaws in the material influences the strength, and thus implicitly assumes that the process of rock specimen deformation and fracture initiation (and thus the stability) is not influenced by size.

Intact rocks

In order to illustrate the size effect the simplest example of an intact rock specimen of cubical shape is examined first. The ultimate stress or strength of this body in uniaxial compression is determined according to LEFM principles by the following condition:

$$\Gamma = \frac{W_{vi} + W_{vm} - W_{vr}}{A_{cr}} \quad (20)$$

where W_{vi} is given by Equation 6, A_{cr} is the total surface area of the critical system of cracks that lead to the failure of the rock body, and W_{vm} is the energy stored in the machine, defined as

$$W_{vm} = \frac{\sigma_{ci}^2}{2k} V_0 \quad (21)$$

where k = machine stiffness (N m^{-2}) and W_{vr} is the residual strain energy stored in the cracked phase of the specimen, which is considered negligible.

Equation 20 means that failure occurs when the load–rock system can deliver the energy required to create a critical crack surface area in the form of localized or diffused deformation in the rock body if

$$A_{cr} = sV_0^{2/3} \quad (22)$$

where s is a constant parameter that relates the geometry of fracturing with the geometry of the rock body. The parameter s is a function of rock microstructure, strength properties, loading conditions and shape of the rock. Then from Equations 6, 20 and 22 it can be shown that

$$\sigma_{ci} = \frac{(2sE'\Gamma)^{1/2}}{V_0^{1/6}} = \frac{\sigma_{c1}}{L^{1/2}} \quad (23)$$

where σ_{c1} is the compressive strength of a unit intact volume, $V_0 = L^3$ for cubical shaped specimens, and $E' = kE/(k + E) = E$ for $k \gg E$. The above dependence of strength on the size of the rock body in compression is predicted by fracture mechanics and has experimentally been confirmed by Johns (1966) for iron ore specimens in uniaxial compression, by Bieniawski (1968) for cubical specimens of coal, by Pratt *et al.* (1972) for diorite, and by Hergert and Unrug (1976) who tested intact siderite specimens in triaxial compression and by Hustrulid (1976). In addition the experiments of all the above researchers revealed that a critical specimen size exists above which the strength of the rock remains constant (asymptotic value), as shown in Fig. 10. This asymptotic character of the size effect was also confirmed by Protodyakonov (1964), Einstein *et al.* (1970) for brittle gypsum–plaster mix specimens in unconfined compression, and by Mandzic (1979) for rock-salt specimens. The initial inverse square root and the subsequent asymptotic character (after some critical value of the size is reached) of the strength–size dependence of brittle fracturing of intact rocks is examined below.

The inverse square root size effect, which characterizes brittle fracture of intact and linearly elastic rocks, can be explained by the fact that the elastic strain energy stored in the rock body is proportional to the volume of the rock, while the surface energy dissipated during fracturing is proportional to the area of the newly created crack surfaces. This also forms the

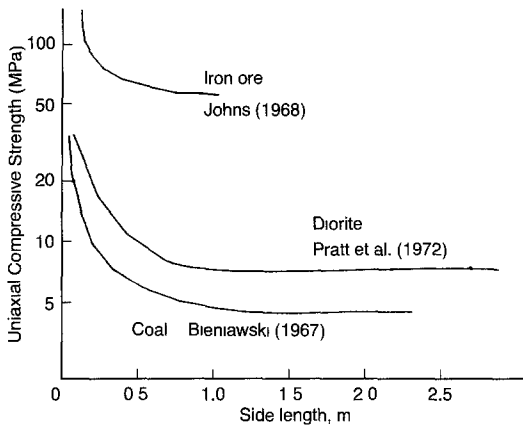


Fig. 10. Relationship between uniaxial compressive strength and size of cubical rock specimens (Bieniawski, 1968)

basis of Berry's (1960) and Cook's (1965) theories. Therefore, in order to investigate the strength–size and stability–size relationships of brittle fracturing of intact rocks, the energy ratio W_A/W_V must be considered. Since this ratio was related by Persson and in this work to the properties of the intact rock, then the size–strength relationship of a given rock can be quantitatively investigated.

The energy ratio W_A/W_V or 'brittleness number' of Equation 7 was first noted by Wawersik (1968, 1970) who describes two different types of post-peak stress–strain behaviour of the rock in compression failure as follows.

- (1) When $W_A/W_V > 1$ then, as is shown in Fig. 11, Class I failure occurs. This is characterized by stable failure in the sense that all the stored elastic strain energy in the rock is converted to surface energy and additional work must be done by the loading system on the rock to reduce its load-carrying capacity until complete failure.
- (2) When $W_A/W_V < 1$ then Class II failure occurs. This is characterized as unstable since energy must actually be removed and the strain decreases, with the softening branch taking on a positive slope (Fig. 11).

A critical state, which divides Class I from Class II – the dashed line in Fig. 11 – represents the case when the elastic strain energy W_V stored within the rock balances the energy W_A required to fracture the rock ($W_A = W_V$).

It can be concluded, therefore, that knowledge of the energy ratio through an experimental estimation of the parameters appearing in Equation 7 can assess the post-peak rock stability behaviour of a linearly elastic, isotropic and intact rock body of given geometry and size subjected to certain loading conditions.

From the above considerations, a 'critical specimen size' exists, above which $W_V > W_A$. This means that the global post-peak behaviour of rock is characterized by Class II instability and there is no size effect as verified by the reported experimental results of several researchers. The critical size of the rock body, L_{cr} , above which there is no size effect, also referred to in the literature as 'representative elemental volume size' (Guisiat and Haimson, 1992), can be found from Equation 7 if we put $W_A = W_V$. In this case

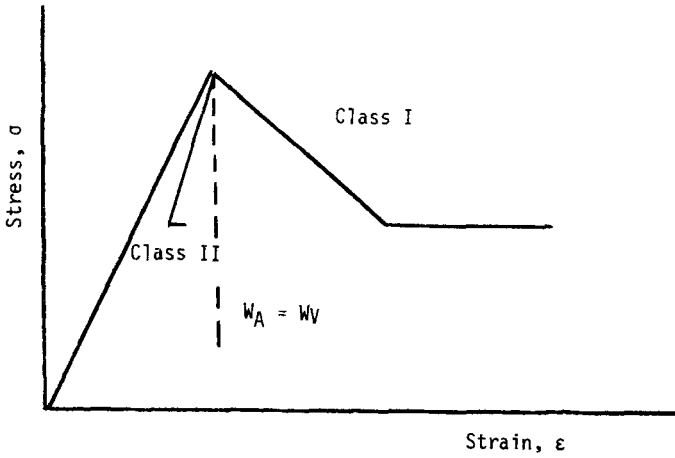


Fig. 11. Stress–strain curves for two classes of failure of a linearly elastic rock (Wawersik and Fairhurst, 1970)

$$L_{cr} = Cr_Y \tag{24}$$

Substituting in the above equation the typical values of parameters $C = 500$ and $r_Y = 0.002$ m for Pendeli marble to 0.008 m for Bohus granite it is found that $L_{cr} = 1\text{--}4$ m. This range of values of L_{cr} obtained from Equation 24 agrees with the range of values shown in Table 7, which were obtained experimentally by various researchers. From the above considerations the scale effect on strength of an intact rock body is described by the relations:

$$\sigma_{ci} = \frac{\sigma_{c1}}{L^{1/2}} \quad \text{for} \quad L < L_{cr} \tag{25a}$$

$$\sigma_{ci} = \frac{\sigma_{c1}}{L_{cr}^{1/2}} = \text{const} \quad \text{for} \quad L \geq L_{cr} \tag{25b}$$

Table 7. Critical rock specimen sizes above which the uniaxial compressive strength approaches asymptotically a constant value

Reference	Rock type	Critical specimen size, L_{cr} (m)
Johns (1966)	Iron ore	1.1
Bieniawski (1968)	Coal	1.7
Pratt <i>et al.</i> (1972)	Quartz diorite	2.5
Pratt <i>et al.</i> (1972)	Coal	4.0
Mandzic (1979)	Rock salt	0.4

The above relationships can be generalized if the fractality of brittle fracture is considered (Chelidze and Gueguen, 1990), by putting

$$A_{cr} = sL^D \tag{26}$$

where D is the Hausdorff–Besicovitch dimension of the crack network, with a lower value of 2

(topological dimension) and an upper value lower than 3 (euclidean dimension). By inserting Equation 26 into Equation 20 it follows that

$$\sigma_{ci} = \sigma_{c1} L^{-(3-D)/2} \quad (27)$$

If the fractal dimension of the three-dimensional network is 2.5, a value which is typical for three-dimensional percolation structures (Aharony, 1986), then the exponent of Equation 27 takes the value -0.25 which was found by Lundborg (1967) to describe the decrease in compressive strength of cylindrical specimens of granite with increasing size.

Discontinuous rocks

In order to extend the above to discontinuous rock, Equations 3, 25a and 25b are considered; that is, euclidean fracture is assumed. From these relations it can be found that

$$\sigma_{cd} = \frac{\sigma_{c1}}{L^{1/2}} e^{-(\beta/L_s)Lf} \quad \text{for} \quad L < L_{cr} \quad (28a)$$

$$\sigma_{cd} = \frac{\sigma_{c1}}{L_{cr}^{1/2}} e^{-(\beta/L_s)Lf} \quad \text{for} \quad L \geq L_{cr} \quad (28b)$$

where β/L_s is a constant dimensionless ratio quantifying the effect of discontinuities on intact rock strength. Both β and L_s are expressed in metres.

From the above relationships it can be seen that:

- (1) one scale effect is due to the fact that the elastic strain energy is converted to surface energy during the fracture process, and
- (2) the other scale effect, which is expressed by the exponential function, is attributed to the presence of pre-existing structural macro-defect surface areas (with size comparable to that of the rock mass) in the rock mass.

Furthermore, there is no scale effect on strength after some critical specimen size L_{cr} (asymptotic character of strength) when there are no pre-existing macro-discontinuities in the rock.

The mode of stability of a discontinuous rock body, which is of great importance in underground mining, can be assessed by using Equation 13. From this equation it can also be seen that, as for strength, one scale effect is due to the conversion of elastic strain energy to surface energy, and the other scale effect, which again is expressed by an exponential function derived in the present experiments, is due to the presence of macro-discontinuity surfaces in the rock. In Fig. 12 stability curves for a rock with f ranging from 0 (intact) to $1 \text{ m}^2/\text{m}^3$ are shown. The rock specimen size was normalized by dividing it with L_{cr} according to the following equation:

$$\frac{W_A}{W_V} = \frac{1}{L/L_{cr}} e^{\alpha(L_{cr}/L_s)f(L/L_{cr})} \quad (29)$$

and $L_{cr}/L_s = 1$ and $\alpha = 0.5$ for the curves in Fig. 12. From this figure it can be seen that the intact rock and the rock with a low f become unstable after some size ($= L_{cr}$ in the first example). Rocks with intermediate f are stable for low and high L but are unstable for L in between, and finally rocks with a high f are stable for all L . This stability behaviour, found

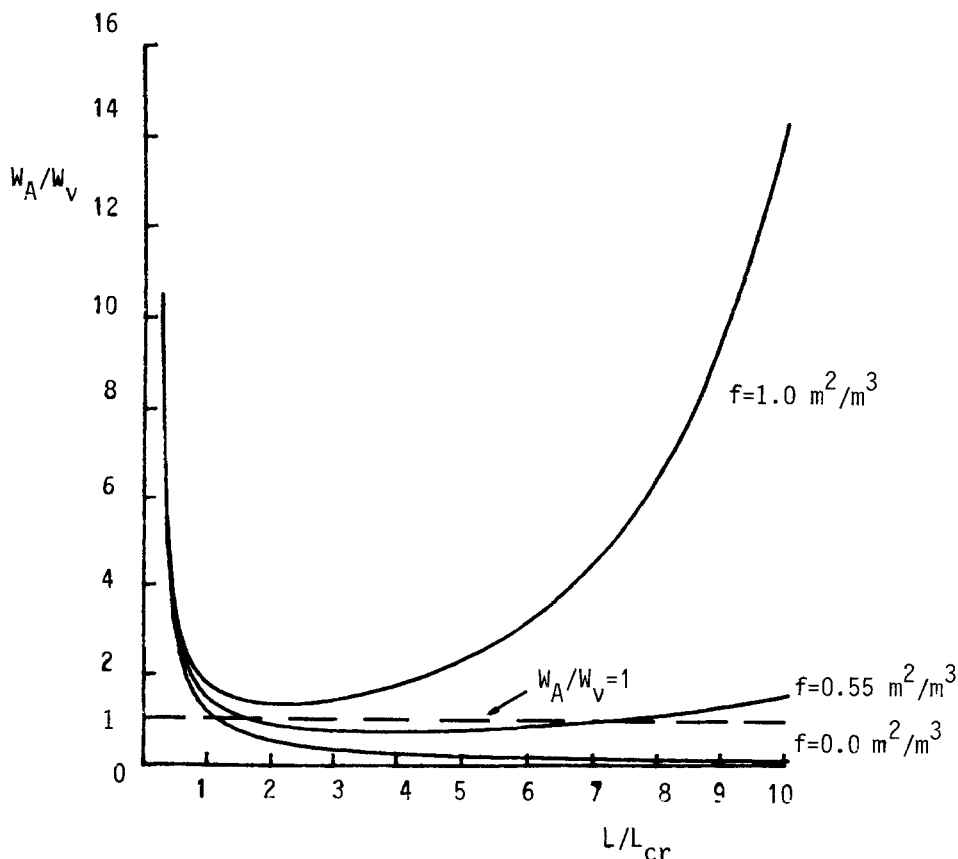


Fig. 12. Effect of normalized specimen size on the stability of a rock specimen in uniaxial compression

from the present uniaxial compression experiments, is similar to the stability function of a precracked beam element found theoretically by Labuz and Biolzi (1991), which has the form

$$\frac{W_A}{W_V} = \frac{\lambda}{12} + \frac{\kappa(1+\nu)}{6\lambda} + \frac{\lambda/5+5}{3\lambda^2} \tag{30}$$

where $\lambda = L/B$ represents the geometric slenderness, L is the beam length (m), B is the beam height (m), κ is a form factor, ν is Poisson's ratio, and B is the independent variable, that is, the size of the specimen.

Conclusions

The effect of visible rock discontinuities (macrocracks) on the strength and on certain fracture energy parameters of Pendeli marble was experimentally investigated. Furthermore, a comparison between laboratory results and field data from *in situ* observations was carried out, considering the rock mass to a first approximation as a linearly elastic material, obeying

the Hoek and Brown failure criterion. In order to predict the *in situ* strength and stability of a rock mass in uniaxial compression, which is of great importance in underground excavations, certain concepts are proposed based on laboratory tests and first principles of LEFM.

References

- Aharony, A. (1986) Percolation, fragmentation, form and flow in fractured media, in *Annals of Israel Physics Society*, Vol. 8, Hilger, Bristol, pp. 77–88.
- Berry, J.P. (1960) Some kinetic considerations of the Griffith criterion for fracture I. Equations of motion at constant force, *Journal of the Mechanics and Physics of Solids*, **8**, 194–206.
- Bieniawski, Z.T. (1968) The effect of specimen size on compressive strength of coal, *International Journal of Rock Mechanics and Mining Science*, **5**, 325–35.
- Bieniawski, Z.T. (1976) Rock mass classifications in rock engineering, in *Proceedings Symposium on Exploratory Rock Engineering*, Johannesburg, Balkema, Cape Town, Vol. 1, pp. 97–106.
- Brown, E.T. (ed.) (1981) *Rock Characterization Testing and Monitoring, ISRM Suggested Methods*, Pergamon Press.
- Brown, E.T. and Hoek, E. (1988) Determination of shear failure envelope in rock masses, discussion, *Journal of Geotechnical Engineering, ASCE* **114**, 371–3.
- Carpinteri, A. (1980) Size effect in fracture toughness testing: a dimensional analysis approach, in *Proceedings International Conference on Analytical and Experimental Fracture Mechanics*, Rome, Italy (eds G.C. Sih and M. Mirable), Sijthoff and Noordhoff, pp. 785–97.
- Chelidze, T. and Gueguen, Y. (1990) Evidence of fractal fracture, *International Journal of Rock Mechanics Science and Geomechanics Abstracts*, **27** (3), 223–5.
- Cherepanov, G.P. (1979) *Mechanics of Brittle Fracture*, McGraw-Hill, New York.
- Cook, N.G.W. (1965) The failure of rock, *International Journal of Rock Mechanics and Mining Sciences*, **2**, 389–403.
- Einstein, H.H., Beacher, G.B. and Hirschfeld, R.C. (1970) The effect of size on strength of a brittle rock, in *Proceedings of the Second Congress of the International Society for Rock Mechanics*, Beograd, pp. 7–13.
- Griffith, A.A. (1921) *Philosophical Transactions of the Royal Society of London*, **A221**, 163–98.
- Guisiat, F.D. and Haimson, B.C. (1992) Scale effects in rock mass stress measurements, *International Journal of Rock Mechanics and Mining Science*, **29** (2), 99–117.
- Herdan, G. (1960) *Small Particle Statistics*, Butterworth, London, pp. 174–5.
- Herget, G. and Unrug, K. (1976) *In situ* rock strength from triaxial testing, *International Journal of Rock Mechanics and Mining Science*, **13**, 299–302.
- Hoek, E. and Brown, E.T. (1980) *Underground Excavations in Rock*, Institute of Mining and Metallurgy, London.
- Hustrulid, W.A. (1976) Review of coal pillar strength formulas, *Rock Mechanics*, **8**, 115–45.
- ISRM (1978) Suggested methods for determining tensile strength of rock materials, *Int. J. Rock Mech. Min. Sci. and Geomech. Abst.* **15**, 101–103.
- Jaeger, J.C. and Cook, N.G.W. (1976) *Fundamentals of Rock Mechanics*, 2nd edn, Chapman & Hall, London.
- Johns, H. (1966) Measuring the strength of rock *in situ* at an increasing scale, in *Proceedings First ISRM Congress*, Lisbon, Vol. 1, pp. 477–82.
- Kaufman, J.G. (1977) Experience in plane-strain fracture toughness testing per ASTM method E399, in *Developments in Fracture Mechanics Test Methods Standardization*, ASTM STP 632, American Society for Testing and Materials, pp. 3–15.
- Kemeny, J.M. and Cook, N.G. (1987) Determination of rock fracture parameters from crack models for failure in compression, in *28th US Symposium on Rock Mechanics*, Tucson, pp. 367–74.

- Krech, W.W. and Chamberlain, P.G. (1972) New techniques for rock fracture energy measurements, in *47th Annual Fall Meeting, Society of Petroleum Engineers of AIME*, San Antonio, Texas, pp. 8–11.
- Labuz, J.F. and Biolzi, L. (1991) Class I versus Class II stability: a demonstration of size effect, *International Journal of Rock Mechanics and Mining Sciences*, **28** (2/3), 199–205.
- Lundburg, N. (1967) The strength–size relation of granite, *Int. J. Rock Mech. and Min. Sci.*, **4**, 269–72.
- Mandzic, E. (1979) Generalization of factors affecting the uniaxial strength of rock material, in *Proceedings Fourth International Congress on Rock Mechanics*, Montreux, Vol. 2, pp. 397–408.
- Nicholson, G.A. and Bieniawski, Z.T. (1990) A non-linear deformation modulus based on rock mass classification, *International Journal of Mining and Geological Engineering*, **8**, 181–202.
- Ouchterlony, F. (1980) *Review of Fracture Toughness Testing of Rock*, SveDeFo Report DS 1980:15, Stockholm, Sweden.
- Persson, P.-A. (1983) Energy in rock fragmentation, in *First International Symposium on Rock Fragmentation by Blasting*, Lulea, Sweden, pp. 777–88.
- Pratt, H.R., Black, A.D., Brown, W.S. and Brace, W.F. (1972) The effect of specimen size on the mechanical properties of unjointed diorite, *International Journal of Rock Mechanics and Mining Sciences*, **19**, 513–29.
- Protodyakonov, M.M. (1964) Methods for evaluating the cracked state and strength of rocks *in situ*, in *Fourth International Conference on Strata Control and Rock Mechanics*, Henry Crumb School of Mines, Columbia University, NY, Addendum.
- Radchenko, L.M. and Mikhailov, V.I. (1970) The grain-size composition of the fragments formed from regularly-shaped specimens in compression tests. *Soviet Mining Science*, No. 1, 41–5.
- Roos, P., Moens, L., De Rudder, J., De Paepe, P., Van Hende, J. and Waelkens, M. (1988) Chemical and petrographical characterization of Greek marbles from Pentelikon, Naxos, Paros and Thasos, in *Classical Marble: Geochemistry, Technology, Trade*, Herz, N. and Waelkens, M. (eds) NATO ASI Series, Kluwer Academic Publishers.
- Shukla, A. and Fourney, W.L. (1983) Influence of specimen size and stress field on energy loss during a fracture event, in *Fracture Mechanics: Fourteenth Symposium – Vol. I: Theory and Analysis*, ASTM STP 791, American Society for Testing and Materials, pp. I-51 to I-64.
- Wawersik, W.R. (1968) *Detailed analysis of rock failure in laboratory compression tests*. PhD Dissertation, University of Minnesota.
- Wawersik, W.R. and Fairhurst, C. (1970) A study of brittle rock fracture in laboratory compression experiments, *International Journal of Rock Mechanics and Mining Science*, **7**, 561–75.
- Weibull, W. (1939) A statistical theory of the strength of materials, in *Proceedings of the Royal Swedish Institute for Engineering Research*, Stockholm, **151**, 115–45.
- Underwood, E.E. (1968) Surface area and length in volume, in *Quantitative Microscopy*, Dehoff, R.T. and Rhines, F.N. (eds) McGraw-Hill, New York, pp. 77–127.

Appendix A

The total surface area A of newly created fractures is defined by Herdan (1960) as:

$$A = KV_0 \sum_i \left[\frac{W_i}{x_i} \right] - A_p \quad (\text{A1})$$

where K is the geometric shape factor of fragments created during fracture [see Table A1 (Herdan, 1960)], V_0 is the initial volume of the test block (m^3), W_i is the weight fraction over a certain size interval, x_i is the average size in that interval (m), and A_p is the total area of artificial discontinuities in the specimen (m^2).

The geometry of the rock fragments produced after each compression test was characterized numerically through digitization of photographs, using a computer program which calculated the

minimum and maximum dimensions of each digitized fragment, and the assumption that $B=T$ (invisible dimension of fragments since photographs are two-dimensional) according to Table A1.

Table A1. Dependence of coefficient K on the geometric shape of rock fragments

$(L \times B \times T)^a$	Sphere	Cube	$4 \times 2 \times 1$	$6 \times 3 \times 1$	$10 \times 5 \times 1$
K^b	6.0	8.3	14.0	19.0	29.0

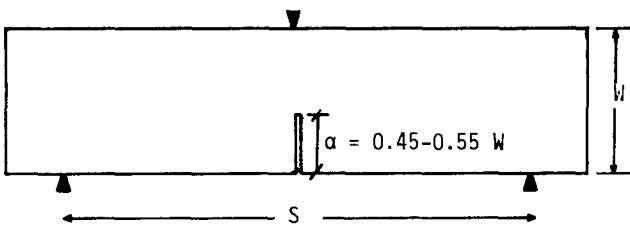
^a L =length (maximum dimension), B =breadth (minimum dimension) and T =thickness of each fragment.

^b $K = [1.57 + C(a/m)^{4/3}(n+1)/n]/a/mn^{1/2}$, where a and C are angularity constants taken as 0.43 and 3.1 respectively, $m = B/T$ and $n = L/B$.

This analysis showed that the ratio n has a mean value of 1.6 and the ratio m is assumed to have a value of 1. According, therefore, to Table A1 the value of the coefficient K is equal to 9.4. Also, the initial volume of each rock specimen V_0 was equal to $0.06 \times 0.06 \times 0.08 \text{ m}^3$ or $2.88 \times 10^{-4} \text{ m}^3$. Therefore the new surfaces created in each test block until complete failure can be established by sieve tests and from Equation A1. Any cracks visible to the eye which were present in relative large fragments and were not considered by Equation A1 were measured separately and added to those estimated by the same equation.

Appendix B

The test procedure for plane strain fracture toughness K_{IC} determination is standardized by the American Society for Testing and Materials (ASTM) (Kaufman, 1977). In bending tests under three-point loading on single edge-notched specimens, as is shown in Fig. B1, the expression for K_{IC} is



specimen thickness = B

Fig. B1. Specimen geometry tested

$$K_{IC} = \frac{PS}{BW^{3/2}} \left[2.9 \left(\frac{\alpha}{W} \right)^{1/2} - 4.6 \left(\frac{\alpha}{W} \right)^{3/2} + 21.8 \left(\frac{\alpha}{W} \right)^{5/2} - 37.6 \left(\frac{\alpha}{W} \right)^{7/2} + 38.7 \left(\frac{\alpha}{W} \right)^{9/2} \right] \quad (B1)$$

where P is the peak or ultimate load on the specimen (N), S is the support span (m), B is specimen thickness (m), W is specimen depth (m), and α is crack length or notch depth ($=0.45-0.55 W$) (m).

Fracture tests were conducted on three-point single edge-notched bend Pendeli marble specimens of thickness $B=99.5 \text{ mm}$, depth $W=51 \text{ mm}$ and notch depth $\alpha=28.5 \text{ mm}$, in an ELE bending machine

(type EL-33-604) of support span $S=180$ mm. The notches were 3 mm wide. The peak load P was obtained for each beam and the average was $P=6.56$ kN with a standard deviation of 0.8 kN. The fracture toughness K_{IC} has been evaluated from Equation B1 to be $1.03 \text{ MN m}^{-3/2}$. Since

$$\gamma = \frac{1}{2} \frac{K_{IC}^2}{E} \quad (\text{B2})$$

and $E=12$ GPa for Pendeli marble, then

$$\gamma = 44 \text{ J m}^{-2}$$